

## RESEARCH ARTICLE

# Mechanical processing via passive dynamic properties of the cockroach antenna can facilitate control during rapid running

Jean-Michel Mongeau<sup>1,‡</sup>, Alican Demir<sup>2</sup>, Chris J. Dallmann<sup>3,\*</sup>, Kaushik Jayaram<sup>3</sup>, Noah J. Cowan<sup>2</sup> and Robert J. Full<sup>3</sup>

**ABSTRACT**

The integration of information from dynamic sensory structures operating on a moving body is a challenge for locomoting animals and engineers seeking to design agile robots. As a tactile sensor is a physical linkage mediating mechanical interactions between body and environment, mechanical tuning of the sensor is critical for effective control. We determined the open-loop dynamics of a tactile sensor, specifically the antenna of the American cockroach, *Periplaneta americana*, an animal that escapes predators by using its antennae during rapid closed-loop tactilely mediated course control. Geometrical measurements and static bending experiments revealed an exponentially decreasing flexural stiffness ( $EI$ ) from base to tip. Quasi-static experiments with a physical model support the hypothesis that a proximodistally decreasing  $EI$  can simplify control by increasing preview distance and allowing effective mapping to a putative control variable – body-to-wall distance – compared with an antenna with constant  $EI$ . We measured the free response at the tip of the antenna following step deflections and determined that the antenna rapidly damps large deflections: over 90% of the perturbation is rejected within the first cycle, corresponding to almost one stride period during high-speed running (~50 ms). An impulse-like perturbation near the tip revealed dynamics that were characteristic of an inelastic collision, keeping the antenna in contact with an object after impact. We contend that proximodistally decreasing stiffness, high damping and inelasticity simplify control during high-speed tactile tasks by increasing preview distance, providing a one-dimensional map between antennal bending and body-to-wall distance, and increasing the reliability of tactile information.

**KEY WORDS:** Biomechanics, Neuromechanics, *Periplaneta americana*, Thigmotaxis, Tactile sensing, Control

**INTRODUCTION**

Sensory appendages that project outside the body, such as arthropod antennae and mammalian whiskers, are physical linkages between an organism and its environment. A major challenge for understanding sensorimotor control is to determine how these sensory appendages might be tuned mechanically when operating on a moving body while interacting with the environment. To reveal

general principles of sensory processing in animals, we must possess a more complete characterization of how appendage mechanics condition information flow as the nervous system operates on a mechanically filtered version of environmental stimuli (Sane and McHenry, 2009). This mechanical filtering defines an open-loop transform that must then be integrated within the control system of animals that includes the dynamics of the body. Using a control theoretic framework integrating open-loop sensory-mechanical transfer functions will ultimately allow us to generate hypotheses predicting sensory processing underlying the control of closed-loop behavior (Roth et al., 2014). Connecting neural and mechanical processing of sensory appendages to control of the body remains a challenge not only for biologists, but also for engineers seeking to design tactile probes on agile robots (Staudacher et al., 2005; Solomon and Hartmann, 2006; Lee et al., 2008; Pearson et al., 2011; Mongeau et al., 2013).

The American cockroach *Periplaneta americana* is an ideal system to study sensory-mechanical processing within a control theoretic framework because we possess quantitative models of its running dynamics (Holmes et al., 2006) that have been integrated within closed-loop control models of antenna-mediated escape behaviors (Cowan et al., 2006; Lee et al., 2008). Recent work has begun to reveal the mechanical transform of the antenna. Mongeau et al. (Mongeau et al., 2013) showed that antenna–environment interactions can play a critical role in wall-following control. This study identified that distal hairs on the antenna can interlock with wall asperities. When coupled with forward motion, the interaction between antennal mechanics, locomotion and environment cause the antenna to reconfigure to an inverted J-shape, which influences wall-tracking control (Mongeau et al., 2013). While we now have a better understanding of antenna–environment interactions, it remains unclear how the passive mechanical properties of the antennal flagellum contribute to control during rapid running. Here, we begin to reveal these properties by studying lumped static and dynamic properties of the antenna of *P. americana*. Using antenna-mediated course control in *P. americana* as a behavioral paradigm (Camhi and Johnson, 1999; Cowan et al., 2006; Baba et al., 2010), we can identify different behavioral events during escape where passive mechanics will shape the response of the antenna and affect control, including: (1) free running, (2) initial collision with object, (3) bending due to normal forces from object, and (4) release from object.

When *P. americana* is freely running, its antennae are propelled rapidly through the environment. Rapid movement of the body generates inertial forces at the center of mass that in turn elicit passive movement of the antenna, as it is physically coupled to the body. In the context of insect flight, motion of sensory appendages driven by rapid body motion can elicit neural responses correlated with Coriolis force to help stabilize flight, as in halteres in fruit flies (Pringle, 1948) and antennae in moths (Sane et al., 2007). However,

<sup>1</sup>Biophysics Graduate Group, University of California, Berkeley, CA 94720, USA.

<sup>2</sup>Department of Mechanical Engineering, Johns Hopkins University, MD 21218, USA. <sup>3</sup>Department of Integrative Biology, University of California, Berkeley, CA 94720, USA.

\*Present address: Department of Biological Cybernetics, Bielefeld University, Bielefeld, 33615, Germany.

<sup>‡</sup>Author for correspondence at present address: Howard Hughes Medical Institute, Department of Integrative Biology and Physiology, University of California, Los Angeles, CA 90095, USA (jmmongeau@ucla.edu)

**List of symbols**

$A_b$	cross-sectional area at base
$A_t$	cross-sectional area at tip
$E$	elastic or Young's modulus
$EI$	flexural stiffness
$F$	force applied on antenna
$f_d$	damped natural frequency
$f_n$	undamped natural frequency
$I$	second moment of area
$L$	length of antenna
$M$	moment or torque
$M_p$	maximum peak value of the transient response measured relative to the final, steady-state value
$r$	radius of antenna
$R$	radius of curvature
$r_b$	radius at base of antenna
$r_t$	radius at tip of antenna
$s$	distance from clamp to force application
$t_d$	time for the transient response to reach half of the final, steady state value
$t_p$	time for the transient response to reach the first peak of the overshoot
$t_r$	time for the transient response to rise from 0 to 100% of the final value
$t_s$	time required for the transient response to reach and remain within 5% of the final value
$x, y$	Cartesian co-ordinates
$y_{def}$	deflection of antenna in $y$ direction
$\Delta$	logarithmic decrement
$\zeta_l$	damping ratio based on logarithmic decrement method
$\zeta_{Mp}$	damping ratio based on overshoot method
$\kappa$	curvature
$\lambda_n$	eigenvalue for truncated conical cantilever beam model determined by fixed-free boundary condition
$\rho$	mass density of antenna
$\omega_0$	undamped angular frequency

antennae or halteres in flight experience less direct physical contact with the environment than appendages used during rapid terrestrial locomotion, such as in course control. An ineffectively tuned terrestrial sensory appendage (e.g. an antenna with low damping) could oscillate excessively when driven by body-generated inertial forces. These oscillations could interfere with the sensing task by making it difficult to separate information due to self-motion versus external contact with the environment.

When coming into or losing contact with an object, passive mechanical properties shape the response of a tactile sensor. Without sufficient damping, a tactile sensor could bounce back from an object upon impact and oscillate excessively upon release. A sensor that is too stiff could cause forces to be transmitted to the body and potentially alter its course. While flexibility may be a desirable feature for a sensory appendage, the tactile structures must be stiff enough to support its own weight (Loudon, 2005). A sensor with large moment of inertia (mass  $\times$  length<sup>2</sup>) could affect the dynamic stability of the body, much like a tail (Libby et al., 2012). In brief, poorly tuned passive mechanical properties could have undesirable consequences by introducing extraneous signals into the sensorimotor transform.

After the antenna of *P. americana* makes contact with an object, it remains unclear how forces from objects are transmitted along the antenna and could condition sensory processing. We hypothesized that tuned stiffness of the antenna shaping antennal bending could improve reliability of information during high-speed tactile navigation tasks by pre-neuronal morphological or mechanical processing, as recently demonstrated in rat whiskers for object localization (Bagdasarian et al., 2013). Mechanical processing has previously been hypothesized to play a role in arthropod antennae but has not been demonstrated

explicitly. Specifically, antennal bending properties that include how the point of bend (relative to the base of the antenna) and/or the contact point shift as the antenna bends, have been linked directly to body-to-wall distance discrimination during high-speed wall following (Camhi and Johnson, 1999). As cockroaches (Camhi and Johnson, 1999) and crayfish (Zeil et al., 1985; Sandeman, 1989) move closer to an object, the straight portion of their antenna (region from base of antenna to bend) shortens as the bend 'moves' towards the base and the flagellum's contact point with the wall (relative to the tip) increases. Camhi and Johnson (Camhi and Johnson, 1999) proposed that the point of bend or the contact point could constitute a one-dimensional map along the length of the antenna that could provide a cue to induce a change in body angle, thus a form of morphological or mechanical processing. Here, we hypothesized that the flexural stiffness ( $EI$ ) of the antennal flagellum would enable effective morphological processing. We first approximated  $EI$  of the antenna and then used a physical model (Demir et al., 2010) to test the effectiveness of morphological processing of different stiffness profiles by correlating the point of bend and contact to the body-to-wall distance, a putative control variable for closed-loop control (Cowan et al., 2006). In addition, we hypothesized that  $EI$  could simplify control by regulating preview distance – the distance that the antenna can sense ahead of the body – as our previous control theoretic model predicts that control is simpler with a greater preview distance (Cowan et al., 2006).

To measure the dynamic response of the antenna and relate it to high-speed antenna-mediated course control, we treated the flagellum as a cantilever beam and measured the time course of passive recovery to biologically relevant deflections. We hypothesized that the flagellum would have a small recovery time to allow the antenna to rapidly recover its original shape (hence preview distance) to respond to impending obstacles. We further hypothesized that the antenna would be highly damped to minimize sensory signal contamination caused by macro-vibrations induced by body dynamics during free running and slipping following loss contact with an object. Finally, to simulate high-speed collisions of the antenna with objects, we developed an impulse-like perturbation and measured the recovery kinematics of the flagellum. We hypothesized that the properties of the collision event would approach a perfectly inelastic collision, so that the flagellum would effectively stick to the object, thereby improving the reliability of tactile information in the running animal by reducing inertial forces on the antenna.

**RESULTS****Flexural stiffness of the antenna decreases exponentially from base to tip**

Geometrical properties were obtained from male *P. americana* antennae *ex vivo*. We determined the radius of the antenna and approximated the second moment of area, a determinant of flexural stiffness that can predict the resistance to bending of the antenna along its length. From  $N=10$  animals (body mass=0.81±0.12 g; mean  $\pm$  s.d. unless otherwise specified; six right antennae, four left antennae), we determined a mean flagellum length of 47.16±3.97 mm and a mass of 0.0023±0.0001 g (Fig. 1A). The length of annuli remained constant until about the 30th annulus from the base (~20% flagellum length), after which there was a marked increase in annulus length up to the 80th annulus (~60% flagellum length) followed by a plateau (Fig. 1B). This sigmoidal increase in annulus length is consistent with a previous study by Kapitskii (Kapitskii, 1984). The number of annuli ranged between 134 and 152 with a median of 146. When averaged across individual animals, the flagella had a base radius of 0.22±0.01 mm, whereas the tip was over four

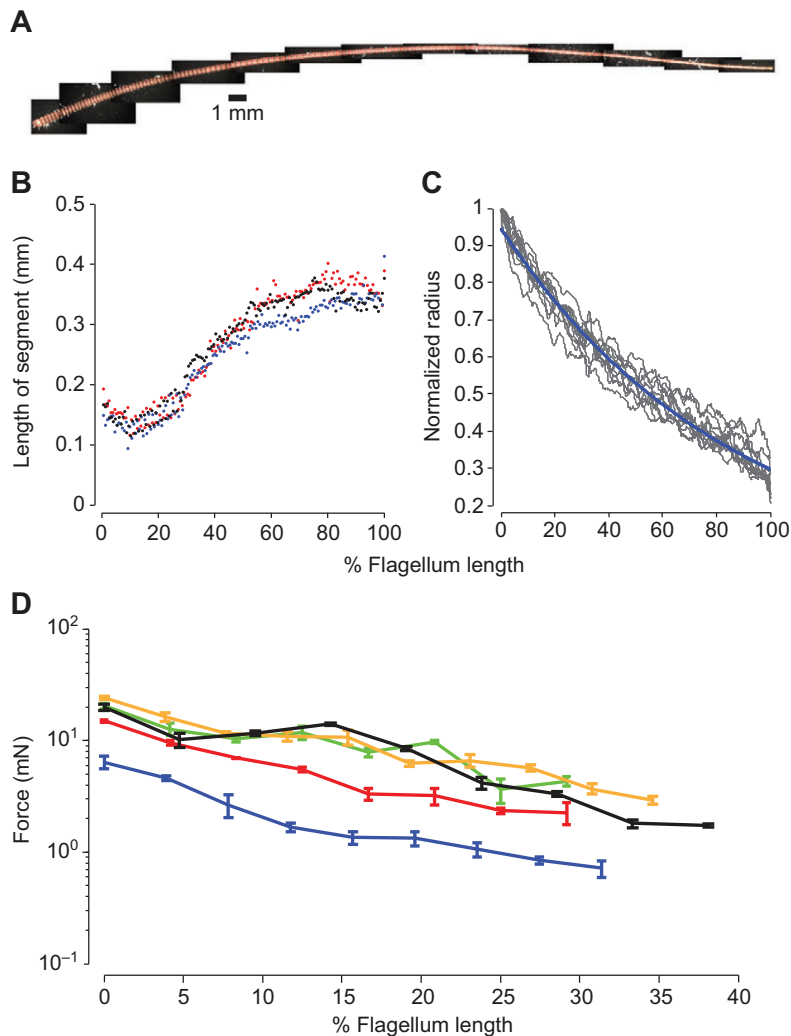


**Fig. 1. Flagellum geometry and resistance-to-bending force.**

(A) High-resolution image of flagellum reconstructed from multiple frames (dark boxes). (B) Length of annuli measured. The length of annuli increased from base to tip, with a transition near 20% of the flagellum length. For clarity, three flagella out of ten are shown using different colors. (C) Variation in normalized radius along the length for 10 animals. The radius decreased exponentially from base to tip. Using a logarithmic model (blue line), all slopes are significantly different from 0 with  $\alpha=0.01$ . (D) Log of resistance-to-bending force versus distance from base for five flagella bent 1 mm laterally (different colors are different antennae than presented in A). The force exponentially decreased from base to tip. Using a logarithmic model, all slopes were significantly different from 0 with  $\alpha=0.01$ .

times finer with a radius of  $0.05 \pm 0.01$  mm. In contrast to a perfect cone, the radius decreased exponentially towards the tip (Fig. 1C). An exponential model ( $\alpha e^{\beta x}$ ;  $\alpha=0.95$ ,  $\beta=-0.012$ , where  $\alpha$  and  $\beta$  are free parameters) captured 94.7% of the variance in normalized radii across individuals [range 95–97% per individual; root mean square error (RMSE)=0.044;  $N=10$ ]. In contrast, a linear model captured less of the variance (91.9%; range 92–96% per individual; RMSE=0.054;  $N=10$ ), with larger residuals particularly near the base and tip of the antenna. We thus approximate the radius of the antenna along its length with an exponential model rather than a linear model. The observed non-linear change in radius is consistent with previous morphometric measurements of the antenna of *P. americana* by Kapitskii (Kapitskii, 1984). From our measurements of the radii, we estimated an upper bound of the second moment of area using Eqn 1 (see Materials and methods). Since the second moment of area at the tip ( $9.48 \times 10^{-18} \text{ m}^4$ ) is three orders of magnitude lower than at the base ( $2.06 \times 10^{-15} \text{ m}^4$ ), this gives us some assurance that the flexural stiffness  $EI$  is determined primarily by geometry. The decreasing flexural stiffness profile of the antenna is consistent with other measurements in tapered arthropod antennae, including the crayfish *Cherax destructor* (Sandeman, 1989) and *Procambarus spiculifer* (Taylor, 1975).

To determine whether the elastic modulus  $E$  also changes along the length and thus affects our estimate of the flexural stiffness profile, we performed static bending experiments on the flagellum

of  $N=5$  adult male *P. americana* (body mass= $0.97 \pm 0.15$  g; antenna length= $4.82 \pm 0.39$  cm; three left antennae, two right antennae). As predicted from our approximation of the second moment of area estimated from our measurements of the radius of the flagellum, the bending resistance of the antenna was greater at the base than at more distal positions (Fig. 1D). We found an exponential decrease in resistance-to-bending force as a function of distance from the base. We found that all slopes were significantly different from 0 ( $t$ -test,  $P < 0.01$  for all animals) after applying a logarithmic transformation. We found no statistically significant effect of plane (lateral versus medial) on the resistance-to-bending forces after including the continuous covariate distance and random factor animal using a logarithmic transformation of force (mixed effect model:  $F=0.04$ , d.f.=1,  $P=0.847$ ). Solving for  $EI$  using a 2D Euler–Bernoulli model (Eqn 2; see Materials and methods) yielded a mean of  $5.78 \times 10^{-9} \pm 4.73 \times 10^{-9} \text{ Nm}^2$  (median= $4.31 \times 10^{-9}$ ; 25% quartile= $2.00 \times 10^{-9}$ ; 75% quartile= $8.34 \times 10^{-9}$ ) over the measured length. This estimate is the same order of magnitude as the flexural stiffness reported for the house cricket *Acheta domesticus* – an insect with a flagellar morphology similar to *P. americana* (mean  $EI$  of  $10 \times 10^{-9} \text{ Nm}^2$  for dorsal and ventral directions at 5 mm from the base) (Kellogg, 2007). To determine whether the resistance-to-bending measurements could be explained by geometry alone, i.e. second moment of area, we used our cantilever beam model to estimate how the elastic modulus  $E$  varied along the measured

region of the antennae, applying an upper bound estimate of  $I$  from geometrical measurements. We found that  $E$  was not statistically different for distances along the length even when considering the possible effect of individuals and plane (mixed effect model:  $F=1.14$ , d.f.=1,  $P=0.288$ ). When pooling  $E$  across different measurement distances along the antenna, we estimated a mean elastic modulus of  $6.91 \times 10^6 \pm 4.47 \times 10^6$  Pa (median =  $5.89 \times 10^6$ ; 25% quartile =  $2.87 \times 10^6$ ; 75% quartile =  $1.01 \times 10^7$ ).

### A physical model reveals that decreasing flexural stiffness increases preview distance and enables effective morphological processing

Using the robotic antenna as a physical model to simulate wall following (Fig. 2A), we tested how quasi-static bending of the antenna could mechanically condition information during running. We tested seven different flexural stiffness profiles while sliding the robotic antenna along an angled wall (Fig. 2B). We measured how the joint of maximum angle correlated with the base-to-wall distance to test the hypothesis that antenna mechanics could simplify body-to-wall distance discrimination in cockroaches. Compared with an antenna with a constant stiffness, we found that a decreasing stiffness profile better linearly maps base-to-wall distance and the point of maximum bend, as evidenced by the higher correlation coefficients (Fig. 3, Table 1). For exponentially decreasing stiffness profiles, we observed that the point of bend or greatest curvature is often located closest to the wall, which is consistent with previous studies of the cockroach *P. americana* (Camhi and Johnson, 1999; Cowan et al., 2006; Mongeau et al., 2013) and crayfish (Sandeman, 1989). In the Discussion, we describe how this observation is predicted from mechanics. We found a marginal increase in correlation coefficient between the base-to-wall distance and the point of contact when comparing a constant with a decreasing flexural stiffness. Secondly, we found that a decreasing stiffness profile increases the preview distance. Overall, there was a significant association between the stiffness profile and preview distance (ANOVA,  $F=76.70$ , d.f.=6,  $P<0.001$ ; Fig. 3, Table 1). *Post hoc* analysis revealed that the preview distance was significantly longer for an antenna with a decreasing stiffness profile compared with one with a constant flexural stiffness (Tukey's test,  $P<0.001$  for all comparisons). For decreasing stiffness profiles, the preview distance generally decreased as the antenna base-to-wall distance decreased, which is consistent with previous observations in studies of wall-following *P. americana* in which these animals run closer to the wall as their speeds increase (Camhi and Johnson, 1999; Cowan et al., 2006).

### An antenna rapidly damps large deflections

We evaluated the damping properties of the antenna by treating it as a cantilever beam fixated at one end and free to vibrate at the other. Since fast-running cockroaches hold their antennae relatively still at the base while their flagella bend in response to upcoming perturbations (Camhi and Johnson, 1999; Cowan et al., 2006; Mongeau et al., 2013), we tested intact antennae with immobilized head-scape and scape-pedicel joints, while leaving the flagellum unrestrained. We determined damping properties by measuring the passive return of  $N=5$  intact flagella after a step deflection (body mass =  $0.79 \pm 0.12$  g; flagellum mass =  $0.0022 \pm 0.0001$  g; flagellum length =  $44.74 \pm 2.56$  mm; three right antennae, two left antennae). After an initial step deflection, the flagellum quickly returned to its starting position (Fig. 4A). Accordingly, time courses of the tip displacements showed clear characteristics of an under-damped system as the antenna oscillated with decreasing peak amplitudes. The amplitude decreased to zero rapidly within 100–125 ms and showed two

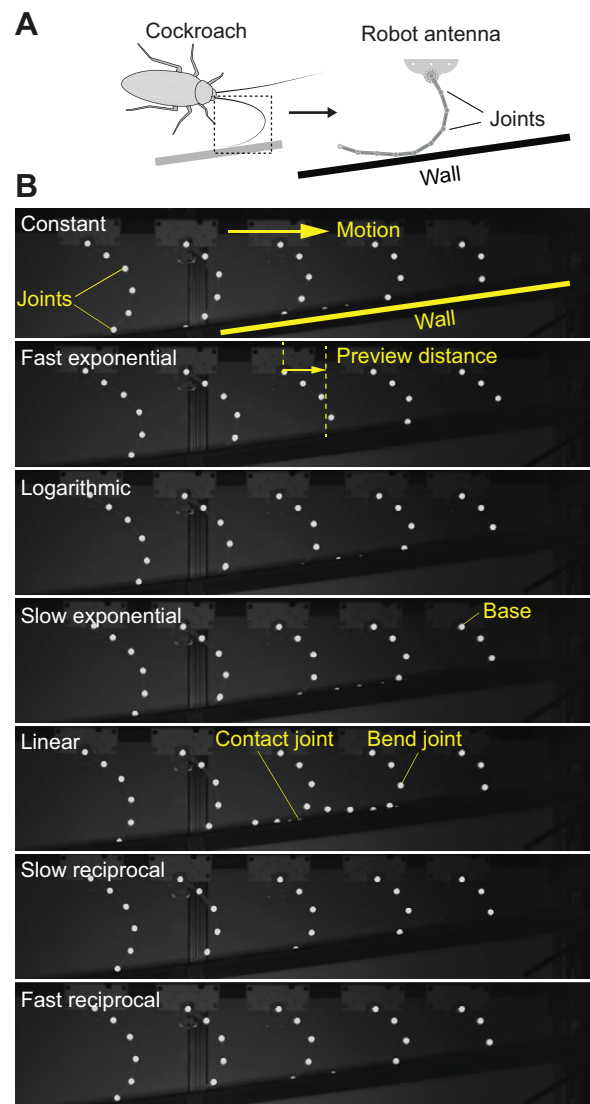


**Fig. 2. Robotic antenna as a physical model to simulate antenna-mediated wall-following.** (A) Diagram depicting a cockroach wall-following along an angled wall (left), with the ipsilateral antenna in a bent-backward configuration (Mongeau et al., 2013), and the corresponding multi-segmented physical model of the antenna (right). (B) Nine-segment physical model of antenna sliding at constant velocity along a smooth, angled wall. We tested seven different stiffness profiles (named in white text on left) and measured how the profiles affected bending properties by tracking the angle of individual joints. The point of bend is the point of greatest curvature computed from individual joint angles. The point of contact is the joint of most proximal contact with the wall. The base is the proximal-most segment from the motorized platform. The preview distance is the distance between the point of wall contact and base. We discovered that the preview distance is greater for decreasing stiffness profiles compared with a constant stiffness profile. The antenna has a total length of 36 cm and each joint can be tuned to a specific stiffness between 0.004 and 0.082 Nm rad<sup>-1</sup>. The antenna traveled a total of 80 cm while the wall distance decreased from 20 to 9 cm.

identifiable overshoots in each trial (Fig. 4B). Both overshoots were statistically significant from baseline across conditions and animals ( $t$ -test,  $P<0.001$ ). Analysis of the average maximum displacements along the length of the unrestrained flagellum revealed that most of the motion occurs at the tip, while the more proximal parts of the flagellum remained stationary and exhibited only small or no overshoot (Fig. 4C). In addition, an increase in initial deflection

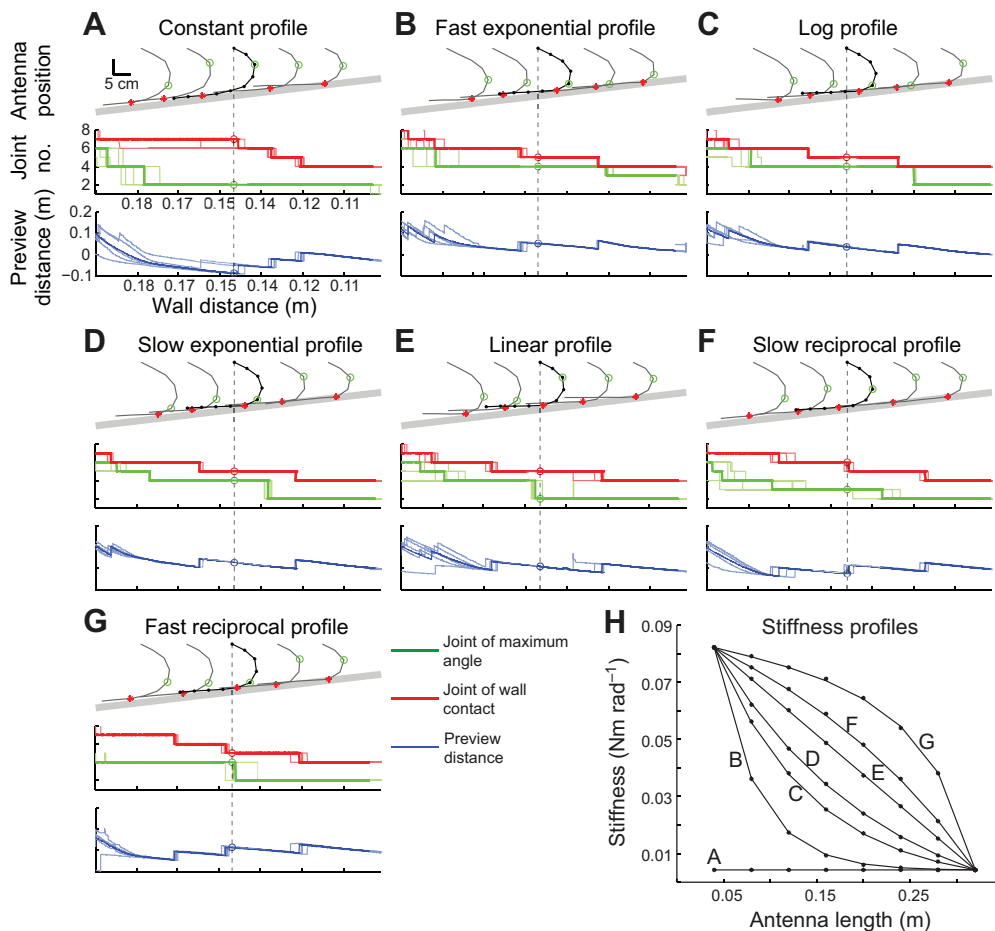


**Fig. 3. A decreasing flexural stiffness profile increases preview distance and better maps body-to-wall distance compared with a constant stiffness profile.** (A–G) Plots of antenna position, joint of maximum angle and wall contact and preview distance for seven different stiffness profiles. For the antenna position plots (top), the gray thick line represents the angled wall. The joints of bend and contact are shown by green, open circles and red asterisks, respectively. The vertical, dashed line represents one frame (dark antenna, top) from a 50 s trial. For the joint no. plot, the red and green lines show the joint of maximum bend and the joint of wall contact, respectively. Thick lines represent one trial matching the trial shown in the top graph. Thin lines represent individual trials. For visual clarity, axes label and scaling are shown for A only but are identical for B–G. These data are summarized in Table 1. (H) Stiffness profiles as a function of antenna length for A–G.

resulted in an increase in maximum displacement. Both the observations of greater tip motion relative to base and sensitivity of displacements to initial deflections are consistent with predictions for an under-damped first-mode vibrating cantilever beam with homogeneous material properties, thus providing some assurance in our measurements of lumped mechanical parameters.

For the two identifiable positive peaks in the time course of the passive recovery, we estimated a damped natural frequency of  $18 \pm 3.0$  Hz and damping ratio  $\zeta_1$  of  $0.52 \pm 0.08$  (Fig. 4D,F). Using the maximum overshoot method (Eqn 5), we estimated a damping ratio  $\zeta_{M_p}$  of  $0.27 \pm 0.07$  (Fig. 4E). Because  $\zeta_1$  and  $\zeta_{M_p}$  were significantly different ( $t$ -test,  $P < 0.001$ ), this suggests that the flagellum transient response is non-linear. Oscillatory time courses were highly consistent within and across animals, and higher mode oscillations were not observed. On average, the flagellum tip rejected 93% of

the initial deflection within the first oscillation cycle (69 ms on average from trough to trough). Deflection directions did not have a significant effect on damped natural frequencies (ANOVA,  $F=0.63$ , d.f.=3,  $P=0.601$ ) and damping ratios (ANOVA,  $\zeta_1$ :  $F=0.28$ , d.f.=3,  $P=0.835$ ;  $\zeta_{M_p}$ :  $F=0.84$ , d.f.=3,  $P=0.477$ ). When taking into account the effect of individuals and initial angles using a mixed effect model, the effect of initial deflection direction on damped natural frequency (mixed effect model,  $F=2.29$ , d.f.=3,  $P=0.097$ ) and damping ratios (mixed effect model,  $\zeta_1$ :  $F=1.31$ , d.f.=3,  $P=0.288$ ;  $\zeta_{M_p}$ :  $F=0.90$ , d.f.=3,  $P=0.450$ ) remained insignificant.

The time characteristics of the response were affected by the initial deflection angle. An increase in deflection resulted in a significant decrease in damped natural frequency (mixed effect model,  $F=88.87$ , d.f.=2,  $P < 0.001$ ) and a significant increase in damping ratios (mixed effect model,  $\zeta_1$ :  $F=4.47$ , d.f.=2,  $P=0.019$ ;

**Table 1. Performance metrics of robotic antenna with different stiffness profiles**

Stiffness profile	Correlation with body-to-wall distance		Preview distance* (cm)	
	Point of bend	Point of contact	Mean $\pm$ s.d.	Median
Constant	0.56 (0.60)	0.91 (0.91)	-2.9 $\pm$ 1.2	-3.0
Decreasing				
Fast exponential	0.83 (0.88)	0.94 (0.95)	4.4 $\pm$ 0.5	4.0
Logarithmic	0.87 (0.88)	0.94 (0.94)	3.5 $\pm$ 0.3	3.2
Slow exponential	0.91 (0.92)	0.94 (0.94)	2.5 $\pm$ 0.1	2.2
Linear	0.86 (0.87)	0.93 (0.94)	1.3 $\pm$ 1.0	0.6
Slow reciprocal	0.84 (0.89)	0.96 (0.96)	0.1 $\pm$ 0.5	0.0
Fast reciprocal	0.86 (0.86)	0.96 (0.96)	-0.6 $\pm$ 0.3	-0.6

Pearson's and Spearman's rank (in parentheses) correlation coefficients are shown. \*Measured from point of attachment of antenna.

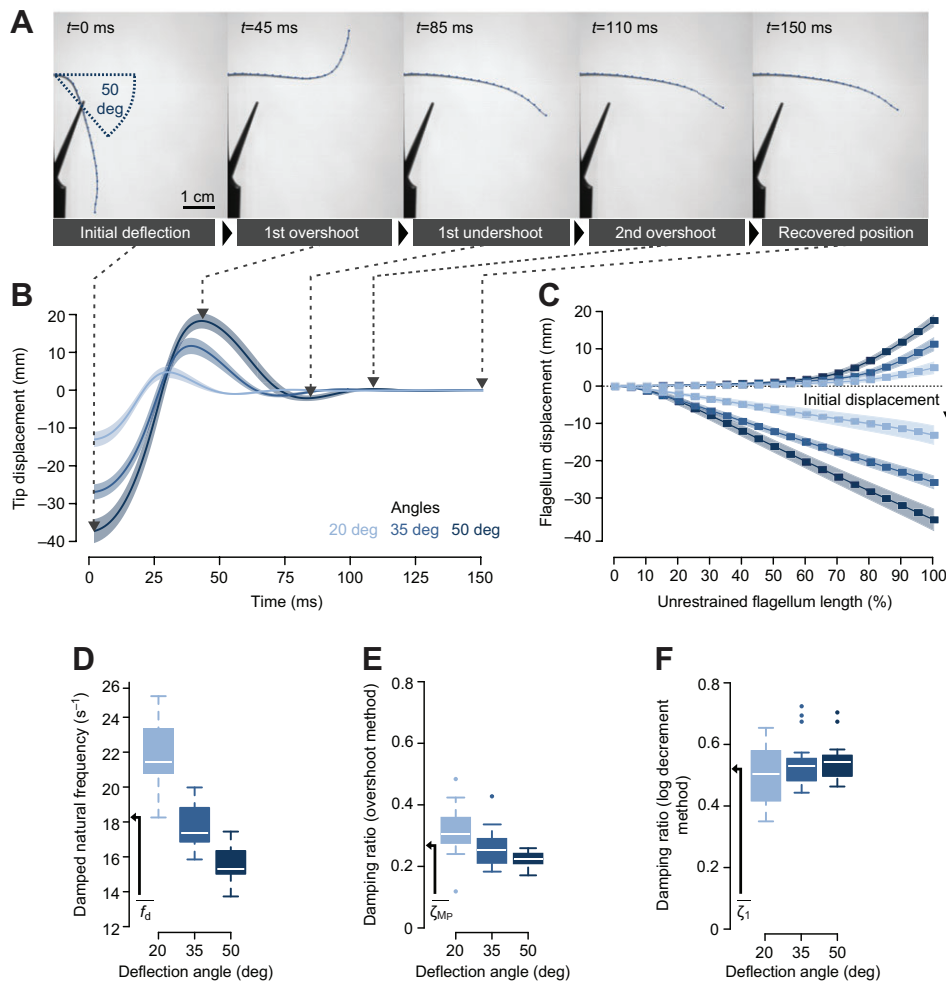


**Fig. 4. Antennal flagellum step deflection response.** (A) Sequence of flagellum recovery from a step deflection of 50 deg with 21 automatically tracked points overlaid in blue. (B) The tip of the antenna recovered rapidly after an initial deflection of 20, 35 or 50 deg and exhibited only two overshoots. Most of the perturbation was rejected within the first oscillation cycle (~70 ms on average). (C) Analysis of the maximum displacement of different parts of the flagellum during recovery revealed large deflections towards the tip, with little-to-no motion transferred at the base. Dark lines represent the mean, and the shaded region is  $\pm 1$  s.d. The under-damped system is characterized by (D) a mean damped natural frequency  $f_d$  of 18 Hz and mean damping ratios  $\zeta_{Mp}$  (E) of 0.27 (based on overshoot method) and  $\zeta_1$  (F) of 0.52 (based on logarithmic decrement method). For box plots, the central line is the median, the bottom and top edges of the box are the 25th and 75th percentiles and the whiskers extend to  $\pm 2.7$  s.d. Outliers are shown as small colored dots.

$\zeta_{Mp}$ :  $F=20.22$ , d.f.=2,  $P<0.001$ ), after accounting for the effect of individuals. We therefore present these pooled data across animals and orientations, but not across angles. Likewise, transient response properties including delay time, rise time, peak time and settling time were dependent on the initial angle (mixed effect model, delay time:  $F=80.46$ , d.f.=2,  $P<0.001$ ; rise time:  $F=81.27$ , d.f.=2,  $P<0.001$ ; peak time:  $F=148.68$ , d.f.=2,  $P<0.001$ ; settling time:  $F=35.51$ , d.f.=2,  $P<0.001$ ) even after including the possible effect of individuals. Maximum overshoot, however, was not strongly dependent on angle (mixed effect model,  $F=3.46$ , d.f.=2,  $P=0.05$ ) when taking into account the possible effect of individuals. Transient response properties are summarized in Table 2.

To independently validate our measurement of natural frequency and give us some assurance in our estimate of (lumped)  $E$ , we evaluated the theoretical natural frequency of a vibrating beam with model parameters obtained from morphological measurements in this study (Eqn 9; see Materials and methods). Our model is based on

analytical results that predict the vibration of tapered, truncated-cone cantilevers (Conway et al., 1964), which have been confirmed experimentally (Georgian, 1965). We chose the boundary condition according to Georgian (Georgian, 1965), who tabulated eigenvalues  $\lambda_n$  in terms of  $(A_t/A_b)^{1/2}$ , where  $A_t$  is the cross-sectional area at the tip of the cone and  $A_b$  the cross-sectional area at the base. We estimated  $\lambda_n$  to be  $\sim 6$  in our experiment by linearly interpolating the tabulated eigenvalues for each  $(A_t/A_b)^{1/2}$ . We used an average value of  $E=6.46 \times 10^6$  Pa, as determined in the static bending experiments. All other model parameters for Eqn 9 were obtained from our geometrical measurements. We estimated an average volume of  $2.60 \pm 0.21$  mm<sup>3</sup>. This measurement of volume is consistent with measurements from Kapitskii (Kapitskii, 1984) who estimated the volume to be 2.1 mm<sup>3</sup> on specimens who had undergone cryofixation and dehydration with ethanol. From our estimate of volume, we calculated an average density of  $0.88 \pm 0.07$  mg mm<sup>-3</sup> across individuals. Using average values for  $r_b$  (0.22 mm),  $r_t$  (0.05 mm),  $L$  (47.16 mm) and  $\rho$  ( $0.88$  mg mm<sup>-3</sup>) as model inputs resulted in a predicted natural frequency of 25 Hz, which falls within the range of natural frequencies obtained in our experiments (15–31 Hz; minimum–maximum). This agreement between theory and experiment gives some assurance that our estimate of  $E$  is of the right order of magnitude and thus that the antenna has an exponentially decreasing stiffness profile.

**The antennal collision response is approximately inelastic**  
Since the antennae are held in front of the body during high-speed running, the antennal tip is likely the first part to contact an object.

**Table 2. Transient responses to antenna step deflections**

	Initial antennal angle (mean $\pm$ s.d.)		
	20 deg	35 deg	50 deg
Delay time, $t_d$ (ms)	15 $\pm$ 3	20 $\pm$ 2	23 $\pm$ 2
Rise time, $t_r$ (ms)	21 $\pm$ 4	27 $\pm$ 3	30 $\pm$ 2
Peak time, $t_p$ (ms)	30 $\pm$ 5	39 $\pm$ 2	45 $\pm$ 3
Maximum overshoot, $M_p$ (%)	43 $\pm$ 15	46 $\pm$ 13	51 $\pm$ 13
Settling time, $t_s$ (ms)	69 $\pm$ 13	76 $\pm$ 10	89 $\pm$ 12

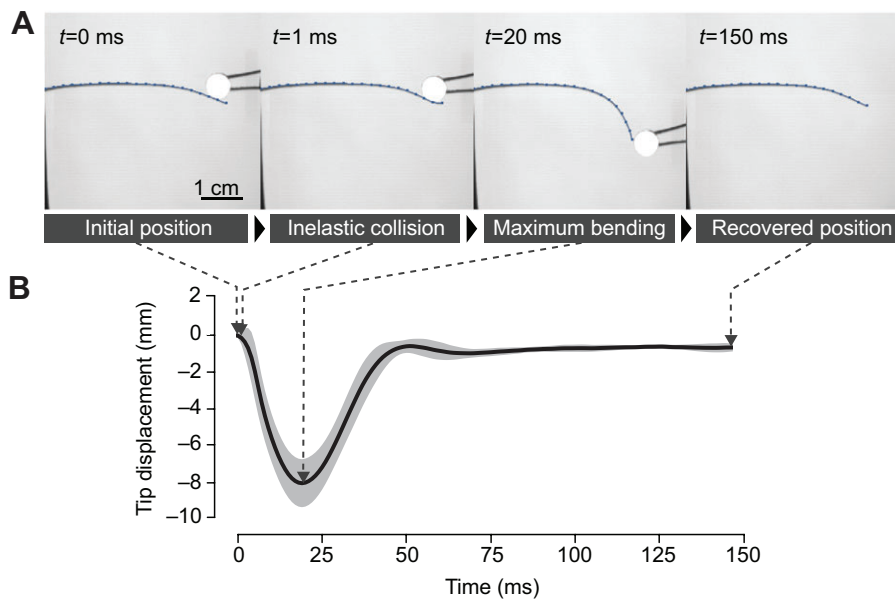


**Fig. 5. Antennal flagellum impulse collision response is approximately inelastic.**

(A) Sequence of flagellar recovery with automatically tracked points overlaid. (B) Time course of tip recovery. The response shows dynamics characteristic of an approximately inelastic collision (at  $t=1$  ms) and antennal bending with peak curvatures close to the site of impact (at  $t=20$  ms). Similar to the step deflection response (Fig. 4), the collision response indicated that motion at the tip was only marginally transmitted to proximal regions. Data were pooled across animals ( $N=5$ ; 10 trials per individual). Dark lines represent the mean and the shaded region is  $\pm 1$  s.d.

During collision avoidance, for instance, the antenna bumps into an object and drives past it. To characterize how the antenna rejects such a perturbation, we analysed the response of the flagellum to an impulse-like collision. We were specifically interested in the dynamic characteristics at the instant of impact and the motion transfer along the flagellum. Accelerated by gravity, the collision object hit the flagellum at a speed of  $60 \text{ cm s}^{-1}$ , similar to average running speeds during wall-following (Cowan et al., 2006). We measured collision dynamics on  $N=5$  intact flagella (body mass= $0.83 \pm 0.13$  g; flagellum length= $49.87 \pm 3.33$  mm; three right antennae, two left antennae). Similar to the step deflections, flagella showed highly consistent collision responses (Fig. 5). After an impulse-like perturbation near the antennal tip, the flagellum remained in contact with the colliding object for up to 20 ms before slipping and rapidly flipping back to its starting position (Fig. 5). At the instant of impact (Fig. 5 at  $t=0$  ms) and throughout the deflection period, there was no observable separation between object and flagellum, which is characteristic of an inelastic collision; the flagellum effectively stuck to the colliding object. Moreover, antennal bending showed peak curvatures close to the site of impact. The point of greatest curvature  $\kappa$  at the instant of maximum deflection (e.g. Fig. 5A at  $t=20$  ms) was always found between 80 and 90% of the unrestrained flagellum length (80%: 12/50 trials; 85%: 18/50 trials; 90%: 20/50 trials), with the perturbation occurring at  $\sim 95\%$  of the unrestrained length. Consistent with the results from the step deflection experiment, all detectable motion was towards the tip.

## DISCUSSION

The present study elucidates the interplay between a dynamic tactile sensory appendage and a rapidly moving body. Here we present how the biomechanical properties of the sensor could be considered tuned for effective tactile-mediated sensorimotor control during high-speed terrestrial locomotion. To define mechanical tuning properties, we analyzed the main tactile sensor of one of the fastest land invertebrate runners – the antenna of the American cockroach, *P. americana* – and characterized its static and dynamic properties.

### Tapering of the antenna increases preview distance and enables morphological processing

During contact, antennal bending is determined by its flexural stiffness and the applied load. From estimates of the second moment

of area and measurements of the resistance-to-bending forces along the flagellum, we determined that the flexural stiffness of the cockroach antennal flagellum decreases rapidly from base to tip (Fig. 1A–C). We found that the forces decreased exponentially, whereas the elastic modulus did not change significantly within the measured length, suggesting that geometrical properties, i.e. tapering, are the main determinant of flexural stiffness (Fig. 1D).

Using a physical model of an arthropod antenna, we tested the hypotheses that a decreasing flexural stiffness profile enables effective mapping of the point of bend and/or point of contact to body-to-wall distance and increases the preview distance. By testing different stiffness profiles, we found that the point of bend maps better to the body-to-wall distance for a decreasing stiffness compared with a constant stiffness profile (Fig. 3, Table 1). The implications for sensing are that antenna mechanics could condition sensing during high-speed tactile navigation with the position of the point of bend acting as a one-dimensional sensory map, as originally proposed in *P. americana* (Camhi and Johnson, 1999) and in the crayfish *Cherax destructor* (Zeil et al., 1985; Sandeman, 1989). Especially during rapid running where neural delays can impose severe constraints on control (Cowan et al., 2006), sensory mapping conditioned by mechanics could be a very desirable feature for simplifying sensing and control. We note that having a tip that is highly flexible could also improve the reliability of tactile flow computation during high-speed running tasks with the antenna better conforming to the shape of obstacles thus allowing more physical contacts, as demonstrated in a previous study using the robotic antenna described here (Demir et al., 2010).

These results are consistent with simple mechanical considerations. As the antenna bends, the point of bend is where the curvature  $\kappa$  will be greatest. For a discretized beam with a force near the tip and with constant stiffness,  $\kappa$  will vary according to  $L^{-1}$  (Eqn 2), such that  $\kappa$  (and therefore the amount of bending) will be greatest where  $I$  is smallest, assuming first-mode bending. Thus more bending should be expected at the tip than at the base. The fact that the point of bend (or point of greatest curvature) is always closest to the wall and appears to ‘move’ considerably as the animal changes its distance to the wall can be attributed to a decreasing second moment of area (assuming  $E$  is constant). In contrast, we would expect the point of bend for a beam or antenna with a constant  $I$  to remain constant. In addition, tapering may mechanically simplify the discrimination of large deflections due

to flow or end loads for underwater robots (Barnes et al., 2001). Under these two conditions, a tapering antenna will produce very different curvature profiles along its length, thus mechanically simplifying discrimination of stimuli. Interestingly, tapering in rat whiskers can improve the reliability of information during slower feature extraction tasks (Hires et al., 2013; Pammer et al., 2013; Solomon and Hartmann, 2011; Williams and Kramer, 2010), and we suspect that similar principles apply to exploratory object localization with antennae.

Using the physical model with tunable flexural stiffness, we found that the preview distance was longer for a decreasing stiffness compared with a constant stiffness profile (Fig. 3, Table 1). To our knowledge, the flexural stiffness of a tactile sensor has never been linked to an animal or robot's preview distance. The practical implication of this result is that a rapidly moving animal or mobile robot equipped with an antenna with decreasing stiffness will detect an obstacle earlier and thus leave more time for an appropriate motor response. For biological systems, particularly when constrained by neural conduction delays which have been estimated to be 20–30 ms from mechanoreception to muscle activation (Camhi and Johnson, 1999; Lee et al., 2008), preview distance is a critical component for stabilizing closed-loop tactile navigation, as demonstrated in control theoretic studies of wall following using simple (Cowan et al., 2006) and dynamically representative (Lee et al., 2008) models of running *P. americana*. These studies determined that the difficulty of closed-loop stabilization is captured by a non-dimensional constant,  $\tau$ , which is inversely proportional to the preview distance,  $l$ . Thus as preview distance increases (while other parameters such as speed remain constant),  $\tau$  decreases, making the system easier to stabilize with feedback. If we assume geometric similarity between our robotic antenna (antenna length=36 cm) and *P. americana* (antenna length=1.3×body length), we would expect the length of our robot body to be ~28 cm, the approximate scale of small hexapedal robots (Saranli et al., 2001). Under simplifying assumptions (see Cowan et al., 2006), preview distance can be measured from the center of mass (COM) of the robot or animal (i.e. about 14 cm would be added to the preview distances listed in Table 1 for a 28 cm robot with COM in the geometric center). Thus for the 'constant' stiffness profile the preview distance would be ~11 cm, while for the 'fast exponential' stiffness profile the preview distance would be ~18 cm or 0.6×body length. This corresponds to a 64% increase in preview distance from the COM, which decreases  $\tau$  by about a factor of 2, thereby making the system significantly easier to control, again assuming geometric similarity and all other parameters being equal. In contrast to our physical model, wall-following *P. americana* can maintain antennal contact distances (measured from COM to point of contact) ranging from ~4 to 5 cm, which is ~1.1–1.3×body length (Cowan et al., 2006). These overall differences in preview distance between model and organism are likely due to differences in friction between the antenna and environment, which has been investigated in previous work (Mongeau et al., 2013), and necessary assumptions and simplifications in the mechanical design of the physical model to test our hypotheses. In summary, we show that biomechanical tuning of the antenna facilitates rapid course control, which can in turn inform the design of wall-following robots moving at multiple body lengths per second.

### The antenna rapidly damps oscillations

The time course of the tip displacement classified the antennal flagellum of *P. americana* as an under-damped system that allows a fast return to its original position after deformation in ~70 ms while exhibiting only two overshoots (Fig. 4B). Interestingly, this average

return time of 70 ms corresponds to almost one stride period during high-speed running (~50 ms) (Full and Tu, 1991). The statistically significant difference in the two independent measurements of damping ratio – based on the maximum overshoot and the logarithmic decrement methods – revealed that the flagellum response is non-linear, quickly settling following a large overshoot (Table 2). The dynamic response showed no signs of directional anisotropy when comparing dorsal, ventral, lateral and medial planes. This directional isotropy corroborates findings in stick insect antennae (Dirks and Dürr, 2011) and is consistent with our static bending results. The variance in frequencies observed in the present study can mainly be attributed to different initial deflection angles. Surprisingly, an increase in the deflection resulted in a significant decrease in the estimated damped natural frequency (Fig. 4E,F). While one would expect a larger deflection to cause an increase in amplitude in a linear system, a change in time characteristics again points towards some non-linearity. Assuming a truncated-cone cantilever beam with geometrical properties similar to that of the flagellum, the model described in Eqn 9 predicted a natural frequency of 25 Hz, which falls within the observed natural frequency range (15.8–31.0 Hz). It should be noted that the lengths of the analysed flagella varied by as much as 12 mm. Although care was taken to select animals with intact antennae, missing distal annuli were common, e.g. due to aggressive behavior with conspecifics. Nevertheless, the dynamic responses were highly consistent and differences in length did not account for a significant part of the variance found in the tip recovery. The non-linearities observed in the antenna dynamic response are consistent with observations from studies of the flagella of the locust *Locusta migratoria* (Heinzel and Gewecke, 1987), where its free response is dependent on the magnitude of initial displacements. Our measured range of natural frequencies is smaller than the natural frequency measured in the antennae of *L. migratoria* (70–132 Hz) (Heinzel and Gewecke, 1987). This difference is consistent with predictions from Eqn 9 – where the natural frequency is inversely proportional to the length square – as the flagellar length of *L. migratoria* is only 14 mm compared with nearly 50 mm in *P. americana*.

Since the flagella were held rigidly near the base (fixed base, free end boundary condition), which is presumably more stiff than the antenna operating on the animal, measurements of (damped) natural frequencies are upper bounds and measurements of damping ratios are lower bounds. The head-scape, scape-pedicel, and pedicel-flagellum joints may damp some of the motion, though it is unclear at present how the fixed-base boundary condition contributes to overall tip displacements. Activation of muscles attaching to these segments could vary the compliance at the base and hence vary the boundary conditions. Thus active neural control may modify damping and natural frequency. However, studies of wall following suggest little-to-no contribution from basal segments; therefore, it is unclear if active control is present at the base during rapid running, besides tonic muscular activity to maintain antennal angles (Camhi and Johnson, 1999). Additional experiments with unrestrained antennae would be necessary to test the contribution of basal segments. At present, it is difficult to assess how the antenna responds to step-like perturbations in the behaving animal. Specifically, as the dynamics of the body also drive antenna motion towards the tip, it is a challenge to separate passive antenna dynamics from body-driven dynamics during recovery. In fact, preliminary data obtained from 3D tracking of the tip in freely running *P. americana* show maximum dorsoventral displacements of over 2 cm in amplitude, despite the COM having vertical excursions of only 0.3 mm (Full and Tu, 1991).

### Antennal collision is approximately inelastic

To understand how the flagellum physically interacts with the environment, we simulated an antenna colliding with an obstacle near running speed. We determined that the flagellum is highly flexible at the tip, with little to no perturbation transmitted to the base when impacting an object (Fig. 5). In accordance with observations from collision-avoidance behaviors such as wall following (Camhi and Johnson, 1999), both step and impulse responses indicate that most of the motion occurs towards distal parts of the antenna. The amount of motion decreases roughly exponentially towards the base, with the proximal regions exhibiting no macro-scale vibrations (Fig. 4C; i.e. vibrations with amplitudes larger than our resolution of 0.1 mm). This result is consistent with our findings showing that the antennae of *P. americana* have a decreasing, non-linear flexural stiffness profile from base to tip. Furthermore, the collision response showed dynamics characteristic of an inelastic collision. The antennal tip did not move away from the colliding object at the instant of impact (Fig. 5A, at  $t=1$  ms), but was dragged along until increased bending caused it to slip and snap back rapidly (Fig. 5A, at  $t=20$  ms). These findings support the notion that *P. americana* does not sense macro-scale antennal deflections at the base, but rather that information may be encoded in the shape of the flagellum itself (Camhi and Johnson, 1999). Along the flagellum, the distal part appears to be critical for sensing. Its flexibility may increase the overall contact area with an object and maintain contact during high-speed running from the instant of impact. This property reduces high-frequency oscillations of the flagellum, which may in turn reduce sensory signal contamination propagating through the mechanosensory array. By showing that the flagellum effectively sticks to objects upon impact, we contend that this can improve the reliability of tactile information in the running animal by reducing inertial forces on the antenna.

### Conclusions

Here we evaluate lumped mechanical properties of the cockroach antenna and provide evidence that passive mechanics may simplify control during high-speed tactile navigation tasks by (1) increasing preview distance, (2) providing a one-dimensional map between antenna bending and body-to-wall distance, (3) damping high-frequency macro-vibrations and associated sensory signal contamination that arise after the antenna loses contact, allowing rapid, passive recovery of the original antennal shape to respond to an impending obstacle, and (4) keeping the flagellum in contact with an object after impact, thereby increasing the reliability of tactile information while isolating the contact event from inertial body motion.

For roboticists seeking to design tactile probes to add new capabilities to mobile robots, choosing mechanical design parameters that integrate with the body remains a challenge. The next generation of agile and multifunctional robots will undoubtedly benefit from building sensors with the body in mind. Our collaborative work transferring biological principles to engineering is informing the design of a statically and dynamically tunable bio-inspired tactile antenna (Demir et al., 2010). In return, this physical model allows us to test biological hypotheses that would otherwise be extremely difficult to test in live, behaving animals.

## MATERIALS AND METHODS

### Animals

Adult male American cockroaches, *Periplaneta americana* (L.), were acquired from a commercial vendor (Carolina Biological Supply Company, Burlington, NC, USA) and housed in plastic cages maintained at a temperature of 27°C. Cockroaches were exposed to a light:dark cycle of

12 h:12 h and given fruits, dog chow and water *ad libitum*. All experiments were conducted at room temperature (25–26°C).

### Geometrical measurements

After sedation of an animal with CO<sub>2</sub> for ~5 min, we cut the antenna at the head-scape joint, and weighed the flagellum to the nearest 0.1 mg. The first few annuli of the flagellum were glued to a microscope glass slide using epoxy to mount it as flat as possible and minimize hemolymph loss. The slide was rigidly mounted on a single axis micro-positioning stage and placed under a microscope with backlighting to maximize contrast of the flagellum against the background. The flagellum was then photographed in overlapping segments of approximately 15 annuli with a high-definition camera (Canon Vixia HF S20, Tokyo, Japan; 3264×2456 pixels) mounted on an optical microscope. Starting at the first flagellum segment, images were taken along the length of the antenna with care taken to ensure overlapping features across images. Frames were calibrated with an objective micrometer with a resolution of 0.010 mm. Single images ranged from 428 to 460 pixels mm<sup>-1</sup> in spatial resolution and were used to manually reconstruct an entire high-resolution image of the flagellum (Adobe Photoshop CS3, Adobe Systems Inc., San Jose, CA, USA). We measured geometrical properties of the flagellum based on a 2D reconstruction using custom-written scripts in MATLAB (The MathWorks Inc., Natick, MA, USA). We first subtracted the background from the composite image and converted it to binary. Detecting the contour and finding the median point along its length then allowed us to approximate the central axis of the flagellum irrespective of its inherent curvature. We applied a spatial moving average filter spanning 400 pixels (~2 mm) to reduce noise associated with annuli intersections.

We estimated the second moment of area  $I$  of the flagellum by assuming a circular cross section, thus:

$$I = \frac{\pi r^4}{4}, \quad (1)$$

where  $r$  is the radius along the length of the flagellum directly measured from high-resolution images. The assumption of a circular cross-section is strongly supported by the morphological studies of Kapitskii (Kapitskii, 1984). While the flagellum is a hollow structure with an inner radius (epithelium) and outer radius (cuticle), this relationship gives us an upper bound on  $I$ . Because both the thickness of the epithelium and cuticle co-vary with the radius of the antenna, our estimates are a good approximation of the upper bound (Kapitskii, 1984).

### Static bending experiment

We built an apparatus to characterize flexural stiffness along the length of the flagellum (Fig. 6A). Cockroaches were first cold-anesthetized for 30 min and weighed. We then fixed neck-lesioned cockroaches onto the edge of a platform using epoxy glue so that the flagellum projected outside the platform surface, unobstructed. This procedure left the antenna auxiliary hearts intact. We fixed the head, scape and pedicel joints with epoxy glue to prevent movement of the antenna during an experiment. The platform was mounted rigidly to a linear micro-translation stage operating in closed loop with a minimum step size of 50 nm (M112.1DG, Physik Instrumente, Palmbach, Germany).

We measured the resistance-to-bending forces generated by the antenna flagellum at different positions along its length, similar to the method employed by Sandeman (Sandeman, 1989) to characterize the mechanical properties of crayfish antennae (Fig. 6A). First, we clamped the antenna using fine forceps while a digital microscope camera (Dino-Lite Premier AD4113TL, AnMo Electronics Corporation, Taipei, Taiwan) was used to visually confirm that the flagellum was held rigidly. We carefully brought a rigid arm attached to a force sensor (Series 300, Aurora Scientific Inc., Ontario, Canada) in contact with the antenna using the micron-resolution stage. The arm was brought in contact as close as possible to the antenna while the measured force remained at baseline. For all experiments, the arm was carefully positioned 1 mm distally from the fixation point of the antenna (Fig. 6A). The first, proximal fixation point was taken five annuli distal from the pedicel-flagellum joint. The force lever was driven perpendicularly into the antenna with a fixed displacement of 1 mm and speed of 2 mm s<sup>-1</sup> using a linear translation stage with submicron resolution (M112.1DG, Physik Instrumente), while forces were sampled at 1000 Hz (Fig. 6A). To minimize

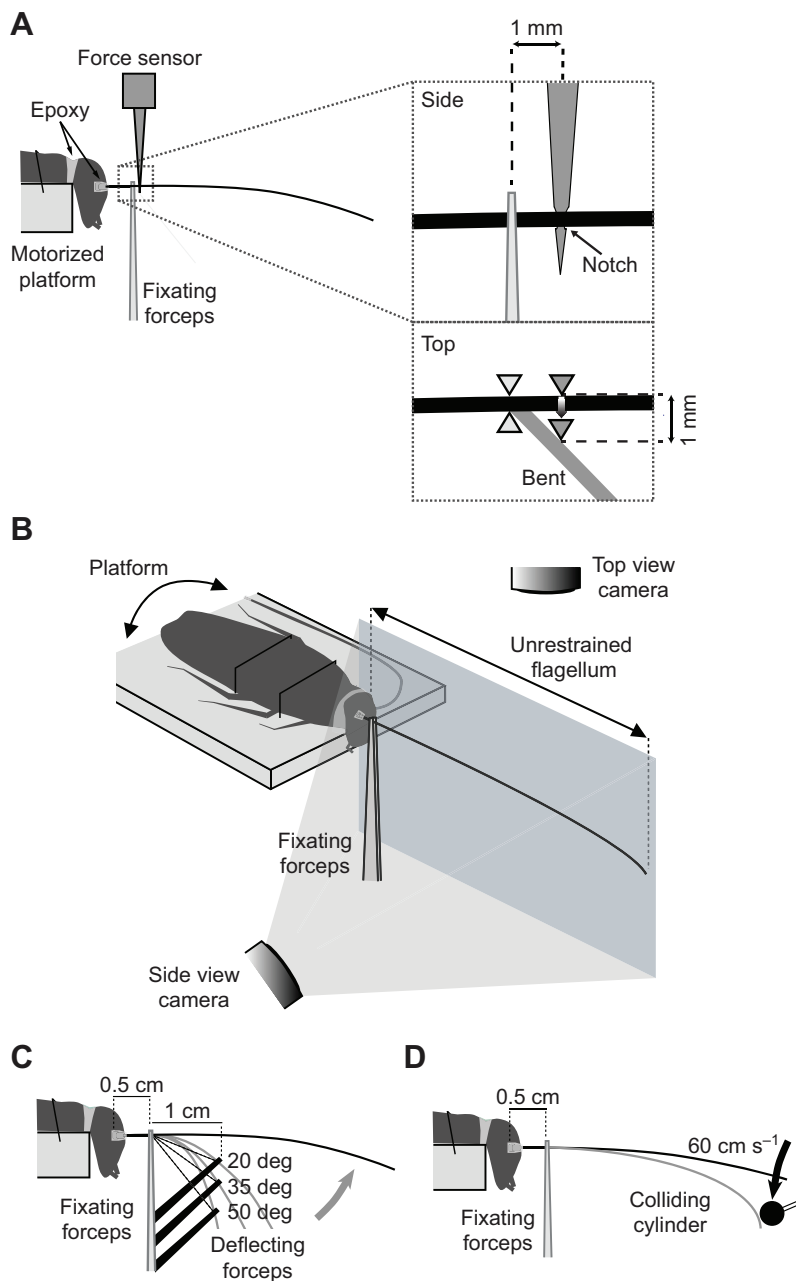


**Fig. 6. Setup for static bending and dynamic response measurements of the flagellum.** (A) Apparatus for determining the variation in flexural stiffness of the antenna. The flagellum was held near the base with a pair of fine forceps. A force sensor 1 mm away from the fixation site mounted on a motorized stage deflected the flagellum laterally (away from the midline) by 1 mm while measuring the resistance-to-bending force. A small notch at the base of the arm of the force sensor prevented out-of-plane motion. This procedure was repeated for different points along the flagellum by moving the platform in steps of 2 mm towards the tip. We immobilized the head, scape and pedicel with epoxy. We imposed lateral and medial deflections. (B) Apparatus for determining the dynamic response of the flagellum. The flagellum was fixated 0.5 cm away from the base with a pair of fine forceps. The head and basal segments were immobilized with silicone (green). Two high-speed cameras recorded horizontal and vertical motions during recovery from either (C) a step deflection or (D) an impulse-like collision. For the step deflection, a second pair of forceps was used to deflect the flagellum to different initial angles (20, 30 and 50 deg). Animals were mounted on a rotatable platform to measure the tip response in the lateral, medial, dorsal and ventral planes. In the case of the collision response, a small cylinder hit the flagellum dorsally at  $\sim 60 \text{ cm s}^{-1}$  near the tip to simulate obstacle contact during high-speed running. Antenna not drawn to scale.

out-of-plane motion, the antenna was positioned within a small groove etched at the base of the arm (Fig. 6A). The 1 mm displacement imposed large angle (45 deg) deflections of the antenna, similar to what an antenna may experience when contacting an object when running. This position was held for 15 s before the lever was returned to its original position. We measured the resistance-to-bending force in steps of 2 mm, which required releasing the antenna and clamping at a new position 2 mm distally from the previous measurement point. We repeated this procedure until measured forces became lower than the 0.3 mN resolution of the force lever, which provided coverage of over one-third of the length of the flagellum from the base. We recorded forces for both the lateral and medial planes and recorded three trials for each position. Only antennae with more than five measurements along the length were included in the final analysis. Raw forces obtained from the static bending experiment were smoothed by convolving a moving average window of 200 ms with the response. For analysis, we recorded the peak force prior to relaxation of the viscoelastic-like response; this corresponds to the time when the force lever reaches its final displacement of 1 mm (Fig. 7).

#### Cantilever beam model

To estimate the order of magnitude and variation of  $E$  along the antenna, we modeled our static bending experimental conditions using cantilever beam theory. Since we imposed deflections of  $\sim 45$  deg in our experiment, we used a 2D Euler–Bernoulli beam model to test our hypothesis that  $E$  did not significantly vary along the antenna. We made estimates of  $E$  by numerical integration, which required approximating:

$$\kappa(x) = \frac{\left| \frac{d^2 y}{dx^2} \right|}{\left[ 1 + \left( \frac{dy}{dx} \right)^2 \right]^{3/2}} = \frac{M(x)}{E(x)I(x)}, \quad (2)$$

where  $\kappa(x)$  is the curvature,  $y$  and  $x$  are the 2D position of the antenna,  $M(x)$  is the moment along the antenna,  $E(x)$  is the elastic modulus and  $I(x)$  is the second moment of area (Timoshenko, 1934). We briefly describe the procedure for numerically solving this equation.

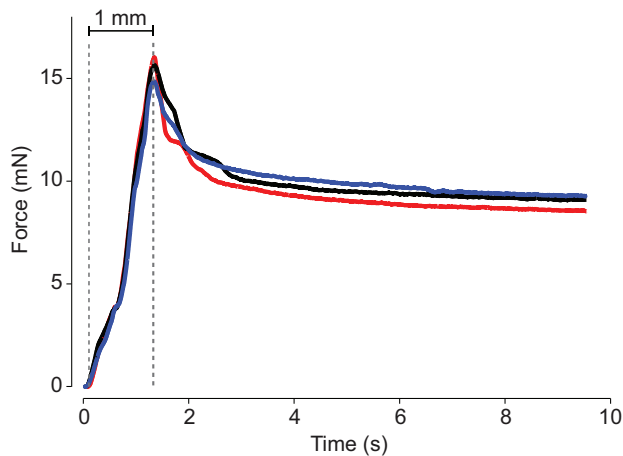


**Fig. 7. Example of force time course for static bending experiment.** Responses exhibit a viscoelastic-like response. Different colored lines represent three different trials at a position of 8 mm away from the base for a fixed lateral displacement of 1 mm applied medially. Gray vertical dashed lines represent the onset and final position of the force lever, thus peak forces represent the time at which the stage reaches 1 mm. Responses are filtered with a moving average filter with a window width of 200 ms.

We adapted the numerical simulation method of Quist and Hartmann (Quist and Hartmann, 2012) to relate the flagellum deflection to the measured force. The model is quasi-static and assumes that the material of the flagellum remains within the elastic limit and that the antenna is inextensible such that the arc length after deflection is equal to the initial length of the flagellum. For the purpose of this simulation, the cockroach flagellum is modeled as a 2D continuously tapering cantilever beam with a circular cross-section (Kapitskii, 1984) under the action of a point force acting perpendicular to the contact at a distance  $s$  measured along the length  $L$  of the flagellum from the clamp position. The simulation computes local curvature of the flagellum at the location of the applied force and then successively calculates changes in the local curvature back to the base of the cantilever (or the clamp position). As a first step, the flagellum was discretized into a series of rigid links connected by elastic torsional springs (Fig. 8). At a given node  $i$ , the curvature,  $\kappa_i$ , is related to the applied moment  $M_i$ , by the equation:

$$\kappa_i = \frac{M_i}{E_i I_i}, \quad (3)$$

where  $E_i$  is the elastic modulus and  $I_i$  is the second moment of area of node  $i$  using the experimentally determined relationship between radius and flagellum length. Using the computed curvature information at each node, the algorithm iterates until the final flagellar shape can be computed passing through the experimentally defined deflection ( $y_{\text{def}}=1$  mm) at the point of force application ( $s=1$  mm). We assume that the elastic modulus within each experimental condition  $[F_i(s), y_{\text{def}}(s)]$  does not change along the length such that  $E_i=E(s)$  is constant for each simulated condition and  $E(s)$  is left as a free parameter to be optimized for obtaining the unique flagellar shape with the least deviation from the desired point  $[y_{\text{def}}(s)]$ . The effect of the continuously changing clamp positions in the experiments is replicated in simulation by using an equivalent flagellum truncated at the clamp position.

### Physical model – robotic antenna

We investigated the mechanical performance of antennae with different flexural stiffness profiles using a physical model of an arthropod antenna (Demir et al., 2010). The robotic platform enabled us to test biological hypotheses while incorporating complex contact interactions that are difficult to simulate computationally (Figs 2, 3). We ran our nine-segment ( $9 \times 40$  mm) robotic antenna along a smooth, angled (8 deg) wall with a constant base velocity of  $16.7 \text{ mm s}^{-1}$  for 50 s per trial. The velocity was sufficiently low for the antenna to stay in a quasi-static state to minimize

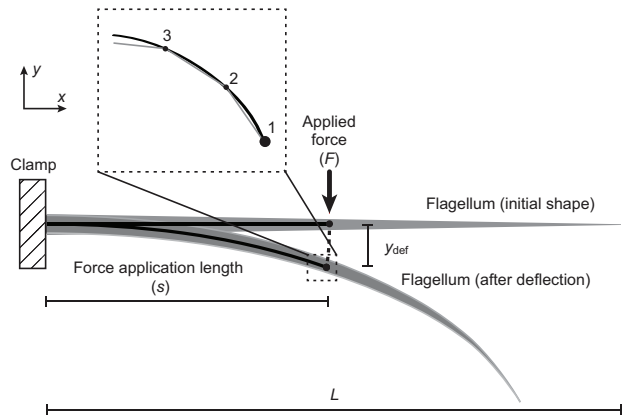


**Fig. 8. Diagram of 2D Euler–Bernoulli beam model.** The flagellum of length  $L$  is modeled as a conical cantilever beam under the action of a point force  $F$  at distance  $s$  from the clamp, with the prescribed deflection  $y_{\text{def}}$ . The flagellum is discretized into a series of rigid links with nodes labeled in the inset. The nodes are evenly spaced along the antenna model with a total of 1001 points. Antenna not drawn to scale.

inertial effects. We set the antenna angle of attack to a biologically relevant value of 30 deg (Camhi and Johnson, 1999) and adjusted the initial wall distance so that the final segment (ninth) was bent backwards (first-mode bending) and in contact with the wall (Mongeau et al., 2013). The antenna traveled a total of 80 cm while the wall distance decreased from 20 to 9 cm. We tested seven different stiffness profiles on the robotic antenna and repeated each trial five times (Fig. 3). We randomized the order of experiments according to the stiffness profile but each replicate for a given profile was done consecutively. We normalized the stiffness distributions for the total length of our antenna (0.36 m) and our available range ( $0.004\text{--}0.082 \text{ Nm rad}^{-1}$ ). For the constant stiffness profile, all joints had the minimum rotational stiffness of  $0.004 \text{ Nm rad}^{-1}$ . All other profiles were decreasing. To sample a spectrum of decreasing mechanical stiffness profiles, we employed the following profiles: linear, exponential ( $\propto e^{-2x}$  and  $\propto e^{-12x}$ ), reciprocal ( $\propto 1/x$  and  $\propto 1/12 \log x$ ) and logarithmic ( $\propto \log x$ ), where  $x$  is the position along the length of the antenna (Fig. 3H). During each trial, we recorded the joint angles at 100 Hz and the position of the antenna base at 30 Hz. For each trial we also captured an overhead video at 30 frames per second for cross-validation, where each joint was marked with retro-reflective markers.

We first tested how stiffness profile affects the discrimination of the point of bend or contact point by computing the correlation coefficient between the points of greatest curvature and contact point with the base-to-wall distance. Secondly, we tested how the stiffness profile affects the preview distance of the antenna, the distance between the distal-most point in contact with the wall and the base of the antenna fixed to the linear platform (Fig. 2B). For analysis, we averaged trials for each condition and averaged the joint angle distributions for every 10 ms interval. For every frame we determined the point of maximum bending and point of contact.

### Dynamics experiments

A cockroach was first anesthetized with ice for 30 min (without direct contact between animal and ice) and mounted *in toto* to a rotatable platform (Fig. 6B). The head and the untested antenna were secured to the platform with dental silicone (Coltene light body, Coltène/Whaledent AG, Altstätten, Switzerland), while both the head–scape and scape–pedicel joints of the tested antenna were immobilized using 5-min epoxy glue after an additional anesthesia with  $\text{CO}_2$  for 1.5 min. Animals were given at least 1 h to recover from the procedure and to ensure that the epoxy glue had fully set. Prior to experimentation, we confirmed that the antenna was intact by lightly probing the antenna and visually confirming the initiation of a stereotypical escape response evidenced by the leg and body twitching.

We fixed the proximal 0.5 cm of the antenna with a pair of fine forceps, leaving the major part ( $\sim 90\%$ ) of the flagellum unrestrained (Fig. 6B,C). A

microscope camera (Dino-Lite Premier AD4113TL, AnMo Electronics Corporation) was used to visually confirm that the flagellum was not clamped too tightly. We recorded the passive recovery from either a step deflection or an impulse-like collision with a high-speed camera (Phantom v10, Vision Research Inc., Wayne, NJ, USA), mounted to view the vertical motion of the flagellum (Fig. 6B). We obtained recordings at 1000 Hz, with a shutter speed of 400  $\mu$ s and a resolution of 10 pixels per millimeter. A second camera (X-PRI, AOS Technologies AG, Baden Daettwil, Switzerland) directly above the antenna (Fig. 6B) additionally recorded the horizontal motion of the flagellum at 250 Hz. These recordings allowed us to discard trials in which motion exceeded the resting, horizontal position of the flagellum by more than  $\pm 15$  deg and thus allowing a small-angle approximation when tracking positions from the side view. The experimental apparatus was mounted on a vibration isolation table. To determine if the ambient airflow in the experimental room affected the trajectory of the tip of the antenna upon deflection and release, we performed a control experiment in which the experimental apparatus was enclosed within an acrylic box. We found that our measurements of natural frequency and damping were not affected by ambient airflow in the experimental room and thus all subsequent experiments were performed in the open.

We characterized the damping properties of the flagellum by analysing the transient response to an initial step deflection (Fig. 6C). The flagellum was deflected manually and held by a second pair of fine forceps 1 cm distal to its fixation site. These forceps were closed above the flagellum. The resulting contact force caused the flagellum to bend in the region between the two pairs of forceps. After a brief hold time of a few seconds, the flagellum was abruptly released and snapped back passively to its starting position. To account for possible directional anisotropies of the flagellum, the animal was rotated such that the flagellum could be deflected ventrally, dorsally, medially and laterally. To further investigate possible effects of initial conditions, the flagellum was deflected to 20, 35 and 50 deg (Fig. 6C). The amount of deflection is well within the biologically relevant range for high-speed collision-avoidance tasks like wall following. To control for the possible effects of order, the sequence of orientations and angles of deflection were varied randomly for each animal. Testing the flagellum in four orientations with three angles of deflection per orientation and three repetitions per angle resulted in a total of 36 trials per individual animal.

### Collision dynamics

To characterize how the antenna rejects a collision with an object during high-speed running, the flagellum was deflected close to the tip (at  $\sim 95\%$  of its unrestrained length) with a 5 mm LED light mounted to a lever arm (Fig. 6D). The use of an LED with a smooth plastic casing allowed contact with negligible friction and created sufficient contrast to clearly identify the flagellar shape in each video frame. The lever arm was released manually and rotated in the sagittal plane. Since the radius of the lever arm was large, the motion during impact following its pendular trajectory was quasi-linear. As the lever arm was multiple orders of magnitude heavier than the flagellum, this experiment simulated a collision of a running animal with a fixed object, in a reverse reference frame. As the step deflection experiment provided no evidence for a directional anisotropy (see Results), the flagellum was deflected only in the ventral direction in the impulse collision experiment. We recorded ten trials per animal.

### Estimating damping properties

We analyzed displacements in response to a step or impulse-like deflection using the video recordings from the side view camera. The position of the flagellum was then automatically tracked for each frame using a custom MATLAB script. Our tracking method allowed us to test the intact flagellum since the tracking algorithm did not require any antennal markers. The script identified the contour of the entire flagellum in each frame after converting images from grayscale to binary. The contour data were smoothed using a spatial low-pass Butterworth filter of second order with a cut-off of 100 pixels ( $\sim 10$  mm). The algorithm then set 21 equally spaced points along the unrestrained flagellum (from the proximal fixation site to the tip, corresponding to 5% length intervals) and determined their displacement relative to the positions prior to deflection. In the case of the step response, the flagellum was partly obscured ( $\sim 5\%$  of the unrestrained length) by the

second pair of forceps during the first few frames; we reconstructed the missing portion using polynomial fitting. To analyse the transient response after a step deflection, we measured the displacement of the tip. At least two distinct overshooting peaks could be identified in each trial and were therefore used to estimate the damping ratio, which determines how much the system oscillates as the response decays toward steady state, and the damped natural frequency, which determines how fast the system oscillates during the transient response. We began our analysis by assuming that the antenna behaved as a linear time-invariant (LTI) system. Specifically, we posit the following, single degree of freedom mechanical model:

$$\ddot{x} + 2\zeta\omega_0\dot{x} + \omega_0^2 = 0, \quad (4)$$

where  $x$  is the displacement of the tip of the antenna,  $\zeta$  is the damping ratio and  $\omega_0$  is the natural (undamped) angular frequency. This model is appropriate assuming we excite a single vibrational mode of the antenna. As we show below, we use multiple distinct methods to estimate model parameters, providing some assurance that this simplified model captures the results of the experiments and allowing us to determine where the experimental results depart from LTI system predictions.

We first measured the damping ratio using the maximum overshoot ( $M_p$ ) method (Ogata, 2003) as:

$$\zeta_{M_p} = \frac{\log(M_p/100)}{(\pi^2 + \log(M_p/100)^2)^{1/2}}, \quad (5)$$

where  $M_p$  is defined as the maximum difference between the transient and steady-state response. To independently determine another damping ratio value, we studied under-damped oscillations of the flagellar response by means of the logarithmic decrement  $\Delta$  (Tongue, 2002). For the first period of oscillation, we calculated:

$$\Delta = \log\left(\frac{A_1}{A_2}\right), \quad (6)$$

where  $A_1$  and  $A_2$  correspond to the amplitudes of the first two peaks, so that in the under-damped case:

$$\zeta_1 = \frac{\Delta}{(4\pi + \Delta^2)^{1/2}}. \quad (7)$$

By comparing the separate measurements of damping ratio, we can assess the linearity of our system as we would expect both measurements to be similar under this assumption. To further characterize the properties of the transient response, we measured standard engineering performance specifications including the delay time  $t_d$ , rise time  $t_r$ , peak time  $t_p$ , maximum overshoot  $M_p$  and settling time  $t_s$  (Ogata, 2003) (Fig. 9).

To compare our results with theoretical predictions from cantilever beam theory, damped natural frequencies  $f_d$ , directly obtained from the peak-to-peak durations of the measured time courses, were transformed into natural frequencies  $f_n$ , assuming linear, second-order damping (Tongue, 2002):

$$f_n = \frac{f_d}{(1 - \zeta^2)^{1/2}}. \quad (8)$$

Here, under the linearity assumption, we would expect estimates of  $f_n$  to be independent of initial conditions, i.e. deflection angle and plane. We then compared the average natural frequency with the natural frequency predicted from a truncated-cone cantilever beam model fixed at one end and free to vibrate at the other (Conway et al., 1964):

$$f_{n,\text{predicted}} = \frac{\lambda_n}{L^2} \left( \frac{EI}{\rho A_b} \right)^{1/2}, \quad (9)$$

where  $\lambda_n$  are tabulated eigenvalues determined by boundary conditions,  $L$  is the length of the cone,  $E$  is Young's modulus,  $A_b$  is the cross-sectional area at the base of the cone,  $I$  is the cross-section moment of area at the base of the cone ( $A_b^2/4\pi$ ), and  $\rho$  is the density of the material.

In addition to the step deflection experiment, the collision response allowed us to obtain a qualitative measure of the dynamic characteristics at the instant of impact (elastic or inelastic collision) and another quantitative

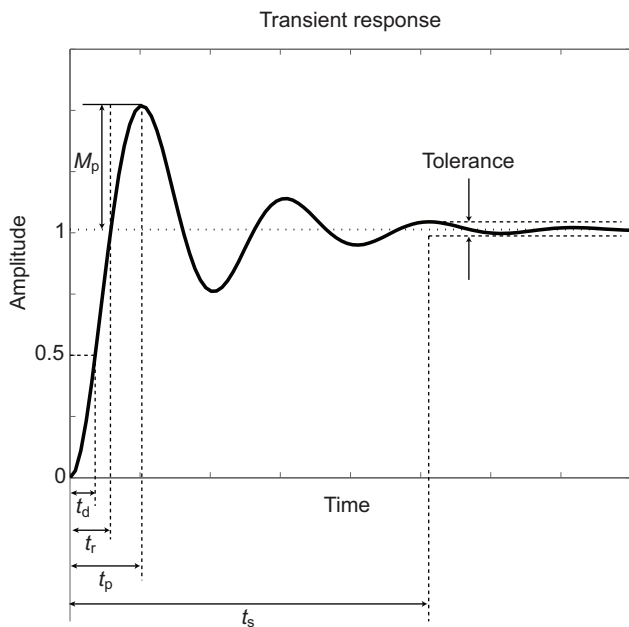


**Fig. 9. Parameters for characterizing the transient response of an under-damped system.**  $t_d$ , delay time;  $t_r$ , rise time;  $t_p$ , peak time;  $M_p$ , maximum percent overshoot;  $t_s$ , settling time.

measure of motion transfer along the flagellum. For the latter, we identified the position of maximum bending by first fitting a polynomial to the automatically tracked points on the flagellum at the time of maximum deflection and then calculating the curvature  $\kappa(x)$  for each point according to Eqn 2, with  $x$  denoting the horizontal co-ordinate of a tracked point in the side view and  $y$  its vertical counterpart from the polynomial fit. The smallest  $\kappa$  along the flagellum corresponds to the position of maximum bending.

### Statistical analysis

We performed all statistical analysis of our data using the statistics toolbox in MATLAB and JMP (SAS, Cary, NC, USA). When including the effect of individual animals for the evaluation of mixed effect models, we treated this variable as a random factor.

### Acknowledgements

We thank undergraduates Anil Mahavadi and Brian McRae for laboratory assistance.

### Competing interests

The authors declare no competing financial interests.

### Author contributions

Conceived and designed the experiments: J.-M.M., A.D., C.J.D., N.J.C. and R.J.F. Performed the experiments: J.-M.M., A.D. and C.J.D. Analyzed the data: J.-M.M., A.D., C.J.D. and K.J. Wrote the paper: J.-M.M., A.D., C.J.D., N.J.C. and R.J.F.

### Funding

This material is based upon work supported by the National Science Foundation (NSF) (Graduate Research Fellowship to J.-M.M.; Integrative Graduate Education and Research Traineeship 0903711 to principal investigator R.J.F. and Traineeship to J.-M.M.); the German Academic Exchange Service (DAAD Promos scholarship to C.J.D.), and the United States Army Research Laboratory (Micro Autonomous Systems and Technology Collaborative Technology Alliance W911NF-08-2-0004 to R.J.F.).

### References

Baba, Y., Tsukada, A. and Comer, C. M. (2010). Collision avoidance by running insects: antennal guidance in cockroaches. *J. Exp. Biol.* **213**, 2294-2302.  
 Bagdasarian, K., Szwed, M., Knutsen, P. M., Deutsch, D., Derdikman, D., Pietr, M., Simony, E. and Ahissar, E. (2013). Pre-neuronal morphological processing of object location by individual whiskers. *Nat. Neurosci.* **16**, 622-631.

Barnes, T. G., Truong, T. Q. and Adams, G. G. (2001). Large deflection analysis of a biomimetic lobster robot antenna due to contact and flow. *J. Appl. Mech.* **68**, 948-951.  
 Camhi, J. M. and Johnson, E. N. (1999). High-frequency steering maneuvers mediated by tactile cues: antennal wall-following in the cockroach. *J. Exp. Biol.* **202**, 631-643.  
 Conway, H. D., Becker, E. C. H. and Dubil, J. F. (1964). Vibration frequencies of tapered bars and circular plates. *J. Appl. Mech.* **31**, 329-331.  
 Cowan, N. J., Lee, J. and Full, R. J. (2006). Task-level control of rapid wall following in the American cockroach. *J. Exp. Biol.* **209**, 1617-1629.  
 Demir, A., Samson, E. and Cowan, N. J. (2010). A tunable physical model of arthropod antennae. In *Proceedings of the IEEE International Conference on Robotics and Automation*, pp. 3793-3798. IEEE.  
 Dirks, J.-H. and Dürr, V. (2011). Biomechanics of the stick insect antenna: damping properties and structural correlates of the cuticle. *J. Mech. Behav. Biomed. Mater.* **4**, 2031-2042.  
 Full, R. J. and Tu, M. S. (1991). Mechanics of a rapid running insect: two-, four- and six-legged locomotion. *J. Exp. Biol.* **156**, 215-231.  
 Georgian, J. C. (1965). Vibration frequencies of tapered bars and circular plates. *J. Appl. Mech.* **32**, 234-235.  
 Heinzel, H.-G. and Gewecke, M. (1987). Aerodynamic and mechanical properties of the antennae as air-current sense organs in *Locusta migratoria*. *J. Comp. Physiol. A* **161**, 671-680.  
 Hires, S. A., Pammer, L., Svoboda, K. and Golomb, D. (2013). Tapered whiskers are required for active tactile sensation. *eLife* **2**, e01350.  
 Holmes, P., Full, R. J., Koditschek, D. and Guckenheimer, J. (2006). The dynamics of legged locomotion: models, analyses, and challenges. *SIAM Rev.* **48**, 207-304.  
 Kapitskii, S. V. (1984). Morphology of the antenna of the male American cockroach *Periplaneta americana*. *J. Evol. Biochem. Physiol.* **20**, 59-66.  
 Kellogg, D. (2007). *Antennal Biomechanics of House Crickets (Acheta domesticus L.)*, 1447112. MA thesis, University of Kansas, Lawrence, KS, USA. Ann Arbor, MI: ProQuest.  
 Lee, J., Sponberg, S. N., Loh, O. Y., Lamperski, A. G., Full, R. J. and Cowan, N. J. (2008). Templates and anchors for antenna-based wall following in cockroaches and robots. *IEEE Trans. Robot.* **24**, 130-143.  
 Libby, T., Moore, T. Y., Chang-Siu, E., Li, D., Cohen, D. J., Jusufi, A. and Full, R. J. (2012). Tail-assisted pitch control in lizards, robots and dinosaurs. *Nature* **481**, 181-184.  
 Loudon, C. (2005). Flexural stiffness of insect antennae. *American Entomologist* **51**, 48-49.  
 Mongeau, J.-M., Demir, A., Lee, J., Cowan, N. J. and Full, R. J. (2013). Locomotion- and mechanics-mediated tactile sensing: antenna reconfiguration simplifies control during high-speed navigation in cockroaches. *J. Exp. Biol.* **216**, 4530-4541.  
 Ogata, K. (2003). *System Dynamics*, 4th edn. Upper Saddle River, NJ: Prentice Hall.  
 Pammer, L., O'Connor, D. H., Hires, S. A., Glack, N. G., Huber, D., Myers, E. W. and Svoboda, K. (2013). The mechanical variables underlying object localization along the axis of the whisker. *J. Neurosci.* **33**, 6726-6741.  
 Pearson, M. J., Mitchinson, B., Sullivan, J. C., Pipe, A. G. and Prescott, T. J. (2011). Biomimetic vibrissal sensing for robots. *Philos. Trans. R. Soc. B* **366**, 3085-3096.  
 Pringle, J. W. S. (1948). The gyroscopic mechanism of the halteres of diptera. *Philos. Trans. R. Soc. B* **233**, 347-384.  
 Quist, B. W. and Hartmann, M. J. (2012). Mechanical signals at the base of a rat vibrissa: the effect of intrinsic vibrissa curvature and implications for tactile exploration. *J. Neurophysiol.* **107**, 2298-2312.  
 Roth, E., Sponberg, S. and Cowan, N. J. (2014). A comparative approach to closed-loop computation. *Curr. Opin. Neurobiol.* **25**, 54-62.  
 Sandeman, D. C. (1989). Physical properties, sensory receptors and tactile reflexes of the antenna of the Australian freshwater crayfish *Cherax destructor*. *J. Exp. Biol.* **141**, 197-217.  
 Sane, S. P. and McHenry, M. J. (2009). The biomechanics of sensory organs. *Integr. Comp. Biol.* **49**, i8-i23.  
 Sane, S. P., Dieudonné, A., Willis, M. A. and Daniel, T. L. (2007). Antennal mechanosensors mediate flight control in moths. *Science* **315**, 863-866.  
 Saranli, U., Buehler, M., Koditschek, D. E. (2001). RHex: A simple and highly mobile hexapod robot. *Int. J. Rob. Res.* **20**, 616-631.  
 Solomon, J. H. and Hartmann, M. J. (2006). Biomechanics: robotic whiskers used to sense features. *Nature* **443**, 525.  
 Solomon, J. H. and Hartmann, M. J. Z. (2011). Radial distance determination in the rat vibrissal system and the effects of Weber's law. *Philos. Trans. R. Soc. B* **366**, 3049-3057.  
 Staudacher, E., Gebhardt, M. and Dürr, V. (2005). Antennal movements and mechanoreception: neurobiology of active tactile sensors. *Adv. Insect. Phys.* **32**, 49-205.  
 Taylor, R. C. (1975). Physical and physiological properties of the crayfish antennal flagellum. *J. Neurobiol.* **6**, 501-519.  
 Timoshenko, S. (1934). *Theory of Elasticity*, 1st edn. New York, NY: McGraw-Hill.  
 Tongue, B. H. (2002). *Principles of Vibration*, 2nd edn. Oxford: Oxford University Press.  
 Williams, C. M. and Kramer, E. M. (2010). The advantages of a tapered whisker. *PLoS ONE* **5**, e8806.  
 Zeil, J., Sandeman, R. and Sandeman, D. (1985). Tactile localisation: the function of active antennal movements in the crayfish *Cherax destructor*. *J. Comp. Physiol. A* **157**, 607-617.